Deep-Sea Research II 56 (2009) 630–639

Contents lists available at ScienceDirect

Deep-Sea Research II

journal homepage: www.elsevier.com/locate/dsr2

Algorithms to estimate the carbon dioxide uptake in the northern North Atlantic using shipboard observations, satellite and ocean analysis data

Melissa Chierici [a,*], Are Olsen [a,b,1], Truls Johannessen [b,1], Joaquin Trinañes [c,e], Rik Wanninkhof [d]

[a] Department of Chemistry, University of Gothenburg, SE-412 96 Göteborg, Sweden
[b] Bjerknes Center for Climate Research, University of Bergen, 5007 Bergen, Norway
[c] Technological Research Institute, University of Santiago de Compostela, Santiago de Compostela, Spain
[d] NOAA/Atlantic Oceanographic and Meteorological Laboratory, Miami, FL 33149, USA
[e] Cooperative Institute for Marine and Atmospheric Studies, University of Miami, 4600 Rickenbacker Causeway, Miami, FL 33149, USA

ARTICLE INFO

Available online 24 December 2008

Keywords:
Chlorophyll *a*
Mixed-layer depth
Surface water
Subpolar gyre
SeaWIFS
MODIS

ABSTRACT

Observations of the surface-water fugacity of carbon dioxide (fCO_2^{sw}) measured during 2005 in the subpolar North Atlantic Ocean (58–62°N, 10–40°W) were used together with *in situ* ocean data and remotely sensed data to develop algorithms to estimate fCO_2^{sw}. Based on multiple regression we found that sea-surface temperature (SST), mixed-layer depth (MLD), and chlorophyll *a* (chl *a*) contributed significantly to the fit. Two algorithms were developed for periods depending on the presence of chl *a* data. The correlation coefficient (r^2) and the root-mean-square deviation (rms) for the best fit in the period when chl *a* was observed (20 March–15 October) were 0.720 and ±10.8 μatm, respectively. The best fit for the algorithm for the period when no chl *a* was present (16 October–19 March) resulted in a r^2 of 0.774 and a rms of ±5.6 μatm. Based on these algorithms we estimated seasonal fields of fCO_2^{sw} and the air–sea CO_2 flux. The estimated net annual CO_2 sink was 0.0058 Gt C yr^{-1} or 0.6 mol C m^{-2} yr^{-1}.

1. Introduction

The North Atlantic acts as one of the more important CO_2 (carbon dioxide) uptake regions ("sinks") of the world's oceans (Takahashi et al., 2002, 2008) due to extensive biological activity and the cooling of the warm Atlantic surface water while it moves northward. However, limited coverage of surface water CO_2 fugacity (fCO_2^{sw}) measurements has restricted our knowledge about the actual role and magnitude of the northern North Atlantic sink (north of 58°N). Volunteer Observing Ships (VOS) have played a major role in improving the temporal and spatial resolution of the temperature (SST) and salinity measurements in the global ocean, as well as of other oceanographic parameters. Recently, some of the ships have been equipped with fCO_2^{sw} sensors, providing high-frequency measurements (1-min intervals) along the ship's track (Cooper et al., 1998; Lüger et al., 2004; Chierici et al., 2006; Olsen et al., 2008). The ultimate goal of the global fCO_2^{sw} observation effort is to constrain regional ocean carbon uptake on seasonal to interannual timescales to about 0.1 Gt C yr^{-1} (1 Gt = 10^{12} kg), which requires the sea–air fCO_2 difference to be determined accurate to between 3 and 20 μatm, depending on ocean region (Sweeney et al., 2002). Given the limitations of the VOS program (ships can only be in a single place at a time), this requires development of robust routines for extrapolation and interpolation of the *in situ* data. Near synoptic data from space-borne sensors have been used to estimate regional fCO_2^{sw} fields through the application of algorithms that take advantage of the correlations between fCO_2^{sw} and remotely sensed variables. In particular, satellite sea-surface temperature (SST) data have been applied in regions like the North Pacific (Stephens et al., 1995), the Equatorial Pacific (Boutin et al., 1999; Cosca et al., 2003), and Sargasso and Caribbean Seas (Nelson et al., 2001; Olsen et al., 2004; Wanninkhof et al., 2007). However, in the northern North Atlantic the SST by itself has not been a good predictor of fCO_2^{sw}, particularly in summer (Olsen et al., 2003). Use of chlorophyll *a* (chl *a*) has been suggested but either no strong relationship has been found (Lüger et al., 2004; Nakaoa et al., 2006) or else they are only valid on short spatial scales (Watson et al., 1991). However, recently Olsen et al. (2008) observed clear correlations between fCO_2^{sw} and both chl *a* and mixed-layer depth (MLD) in the northern North Atlantic. From this, we develop fCO_2^{sw} algorithms applicable to the northern North Atlantic using *in situ* fCO_2^{sw} values, remotely sensed chl *a*, and ocean MLD and SST from an assimilation model. From these relationships seasonal fields of fCO_2^{sw} and sea–air CO_2 flux are created. After a brief description of the hydrography and the study area, we present the remotely sensed and ocean data, and the field measurement program. We use the data set to derive algorithms to calculate fCO_2^{sw} values in the northern North Atlantic. The fCO_2^{sw} algorithms are used to compute weekly fields of fCO_2^{sw}, which are compared with the observed fCO_2^{sw} data and are validated with fCO_2^{sw} measurements

* Corresponding author. Tel.: +46 31 772 2922; fax: +46 31 772 2785.
E-mail address: melissa@chem.gu.se (M. Chierici).
[1] Also at: Geophysical Institute, University of Bergen, 5007 Bergen, Norway.

0967-0645/$ - see front matter © 2009 Elsevier Ltd. All rights reserved.
doi:10.1016/j.dsr2.2008.12.014

from an independent field program. We calculate the sea–air CO_2 flux based on the computed fCO_2^{sw}, and we produce seasonal maps of all study parameters for four seasons.

2. Study area

Olsen et al. (2008) showed that the surface-water fCO_2 characteristics of the shelf regions of the northern North Atlantic, such as the North Sea and the East Greenland Current, differed significantly from the deep ocean regions. Here we focus on the latter region, the area between 10–40°W and 58–63°N (Fig. 1). This area encompasses the Rockall Trough (RTr), and parts of the Iceland Basin (IcB), and the Irminger Basin (IrB), to 40°W. Data from regions with a bottom depth shallower than 500 m were excluded, since they are considered as shelf seas. Our study area is mainly influenced by the relatively warm and saline North Atlantic Current, NAC, which enters the region from the south-west. The water partly continues northward into the Nordic Seas. The rest circulates in the area, with a net movement towards the west, progressively cooling and freshening along its way. These waters are frequently referred as the Subpolar Mode Water (McCartney and Talley, 1982), which mixes with waters of polar origin in the Labrador Sea and forms the coldest and freshest watermass the Subarctic Intermediate Water (SAIW). The SAIW constitutes a large part of the Irminger Basin. The East Greenland Current (EGC) affects the westernmost part in our study area with low-salinity waters from the Arctic Ocean.

3. Data

3.1. Field measurements

The fCO_2^{sw} and SST data were obtained onboard the container carrier M/V *Nuka Arctica* in 2005 (Fig. 1) and are presented by

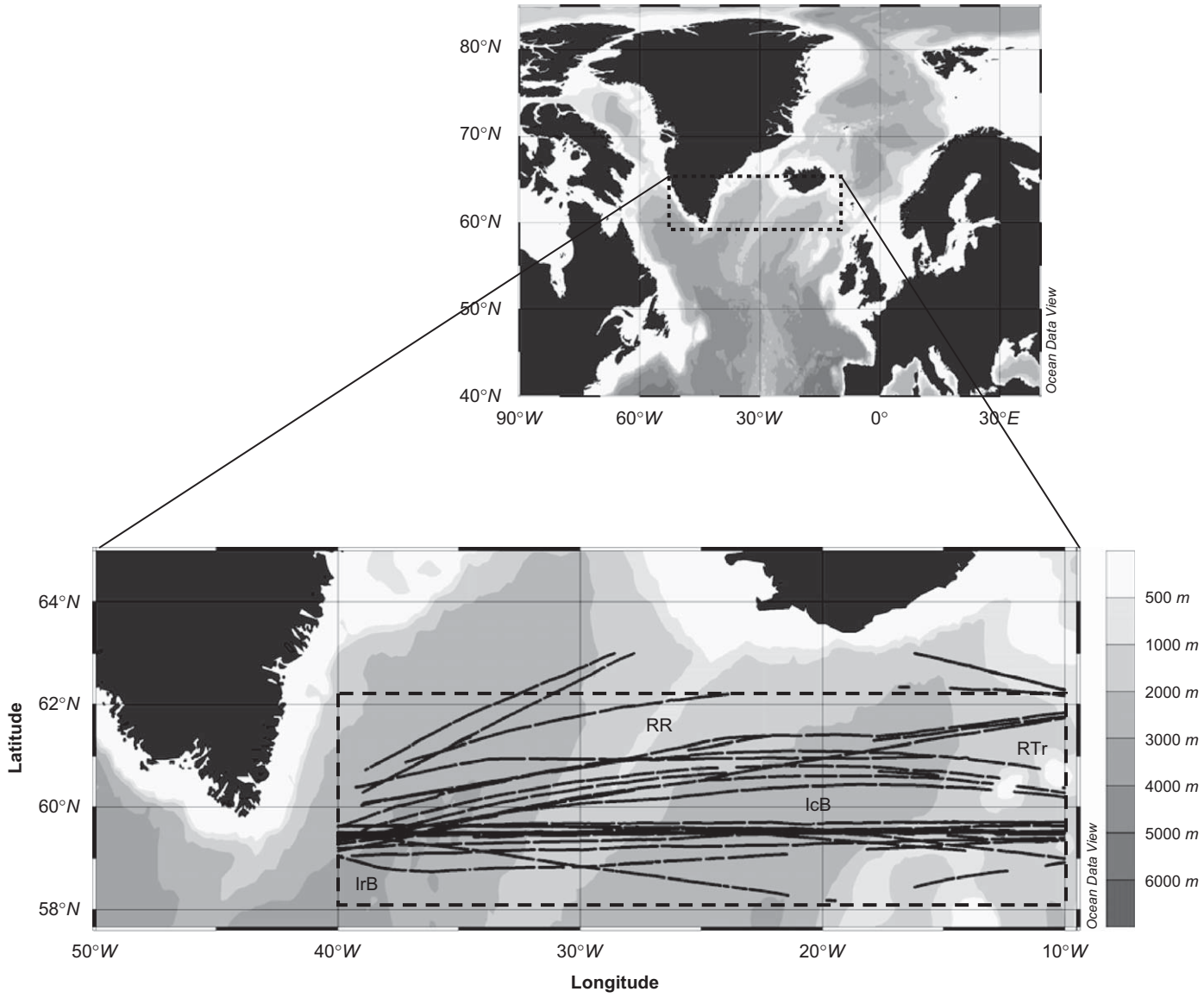

Fig. 1. The location of underway measurements of fCO_2^{sw} and SST used in this study performed onboard the M/V *Nuka Arctica* (here denoted *Nuka*) during 2005. The dashed rectangle indicates the region for which the analysis was performed. In this study we used a total number of 19,048 measurements. IcB and IrB denote the Iceland Basin and the Irminger Basin, respectively. The approximate location of the Reykjanes Ridge (RR) and the Rockall Trough (RTr) are also shown. The grayscale bar illustrates the depth contours in m.

Olsen et al. (2008). In 2005, data were obtained on 27 of the 30 trans-Atlantic crossings, starting January 7 and ending December 3. Generally the ship crosses the Atlantic at roughly 60°N in about 5 days and spends approximately 1 week on the west coast of Greenland and 3 days in Aalborg, Denmark. The data from 2005 have been made publicly available through the Carbon Dioxide Information Analysis Centre (CDIAC) at http://cdiac.ornl.gov/oceans/VOS_Program/nuka_arctica.html. We have used a total of 19,048 data points covering a full annual cycle in the region between 40–10°W and 58–63°N. The fCO_2^{sw} system installed onboard the *Nuka* (since 2004) analyzes the CO_2 concentration in an air headspace in equilibrium with a continuous stream of seawater using a LI-COR 6262 non-dispersive infrared (NDIR) CO_2/H_2O gas analyzer. The system is similar to the instruments described by Pierrot et al. (2008) and Olsen et al. (2008) describes the specific instrumental set-up for the *Nuka*.

3.2. Ocean analysis data

We used the SST and MLD data set obtained from the Forecasting Ocean Assimilation Model (FOAM) of the UK National Centre for Ocean Forecasting (McCulloch et al., 2004). The FOAM data were obtained at http://www.ncof.gov.uk/products.html (McCulloch et al., 2004). This data set was also used in Olsen et al. (2008) study. The data are provided as daily fields on a 1/9° resolution, corresponding to 12.3 km in latitude and 6.2 km in longitude at 60°N. FOAM uses ocean data (salinity, temperature) from several sources; such as Argo profiling floats equipped with salinity and temperature sensors, XBT's (Expendable Bathythermographs), and CTD's (conductivity–temperature–depth-sensors) as well as satellite-derived SST from the Advanced Very High Resolution Radiometer (AVHRR). The daily FOAM data were collocated with the *Nuka* fCO_2^{sw} data with a distance separation of between 0 and 7.8 km, and a mean value of 4 km.

Other SST products from different sensors were tested, such as from the Moderate Resolution Imaging Spectroradiometer (MODIS) and AVHRR. The AVHRR SST data were obtained from the Physical Oceanography Distributed Active Archive Center (PODAAC at the NASA Jet Propulsion Laboratory, Pasadena, CA, at http://podaac.jpl.nasa.gov/poet) The SST data from the MODIS instrument onboard the EOS Terra Satellite were provided by the NASA/Goddard Earth Sciences Distributed Active Archive Center (GES DAAC) at http://daac.gsfc.nasa.gov/. We also used the NOAA Optimum Interpolation (OI) Sea-Surface Temperature V2 (Reynolds et al., 2002). A comparison of the different SST products with the observed SST (from *Nuka*) showed that the SST data generally agree well with the *Nuka* data SST (Table 1). SST from the AVHRR has the smallest offset and the FOAM data the lowest variance from the observations (rms). Since the AVHRR data set is based on less than half of the amount of data as the other SST sources, we consider the FOAM data as more reliable and in best agreement with the observed SST from the *Nuka* data set.

Table 1
Summary of statistics of the ΔSST (remotely sensed/model SST–*Nuka* SST).

	FOAM	AVHRR	MODIS	Reynolds
25th percentile	−0.30	−0.27	−0.43	−0.05
Median residual	0.05	0.09	−0.07	0.20
75th percentile	0.38	0.34	0.21	0.5
Mean	0.02	0.01	−0.09	0.24
rms	0.52	0.57	0.50	0.44
N	19,047	8114	19,047	19,047

N denotes the number of data points used in the analysis. A negative mean denotes a colder SST than the SST measured onboard the *Nuka*, and a positive a warmer. Note that although AVHRR SST agrees well with *Nuka* SST (mean = 0.01), the analysis is based on less than half of the amount of data as the other SST sources. The 25th percentile value (also referred as the lower quartile) indicates the limit where 25% of the residuals fall below the value in the table. Similarly, the 75th percentile (upper quartile) denotes the value where 75% of the residuals fall below.

3.3. Remotely sensed chlorophyll a data

We used the Level 3 merged chl *a* product created and distributed by the Ocean Biology Processing Group (McClain et al., 2006; http://oceancolor.gsfc.nasa.gov) using the satellite measurements from MODIS (OC3 M algorithm), on the Aqua satellite, and the Sea-viewing Wide Field-of-view Sensor (SeaWIFS, OC4V4 algorithm), on the OrbView-2 platform. This product has increased coverage over the single mission products, which is important for these high-latitude regions where cloud cover severely limits the remotely sensed color. The data were collocated with the fCO_2^{sw} data obtained on the *Nuka* with a mean distance separation of 4.0 km and a standard deviation of ±5.6 km.

Satellite-derived chl *a* estimates cannot be obtained in the presence of cloudy skies and during the Polar night. Therefore, few chl *a* data were available for the period before 20 March and after 15 October 2005. This is not a significant issue as during this period chl *a* is not critical for fCO_2^{sw} algorithms, since it is believed that there is little or no biological influence on surface seawater fCO_2^{sw}. Following Lévy et al. (2005), chl *a* values greater than 5 mg m^{-3} were considered unrealistically high and were discarded.

4. Calculations

4.1. Estimation of fCO_2^{sw} algorithms

To develop algorithms describing the fCO_2^{sw} in the surface water we use proxies that represent the main drivers of the fCO_2^{sw} in the northern North Atlantic: temperature, biological processes, and physical mixing. The use of chl *a* as a proxy for fCO_2^{sw} in the northern North Atlantic has been investigated previously. In the present paper algorithms to compute fCO_2^{sw} from SST, chl *a*, and MLD are explored using multiple regression based on the Marquardt–Levenberg routine (Press et al., 1986), which is implemented in the STATISTICA© software. By investigating the fCO_2^{sw} residuals (observed−predicted) in a set of step-wise equations, we analyze the individual contribution of chl *a*, and MLD to the overall fit. This is illustrated in Fig. 2A and B, where the residuals from the regression: $fCO_2^{sw} = 383.01 - 4.288 \times SST + 0.065 \times MLD$, is plotted versus chl *a*. A positive residual means that the predicted fCO_2^{sw} is lower than the observed fCO_2^{sw}, and we observe a correlation between the more negative residuals (fCO_2^{sw} too high) and higher chl *a* values. Next, we study the residuals when chl *a* is included in the algorithm for the equation: $fCO_2^{sw} = 384.82 - 3.579 \times SST - 15.021 \times \text{chl } a + 0.055 \times MLD$; in this case we observe no bias in the residuals versus chl *a* (Fig. 2B). Including chl *a* improved the correlation coefficient (r^2) from 0.62 to 0.68 and decreased the root-mean-square error (rms) from ±14.4 to ±12.8 µatm. The improvement by including chl *a* is similar to the improvement by adding SST, which increased r^2 from 0.62 to 0.68 and decreased the rms from 14.1 to 12.8 µatm. Cubic and/or quadratic functions of SST were tested and showed no significant improvement for the overall rms and r^2 of the algorithm. The inclusion of chl *a* data in the algorithm leads to less biased residuals. This suggests that chl *a* is a useful proxy for the biological CO_2 drawdown during primary production. The same

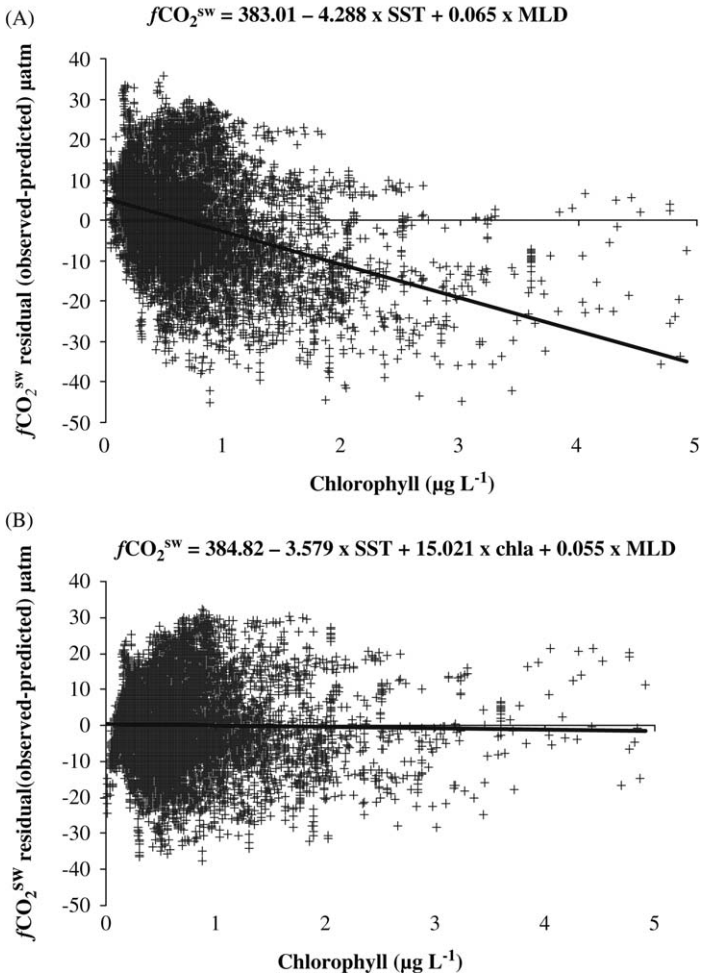

Fig. 2. Residuals (observed−predicted fCO_2^{sw}, µatm) from the equations: (A) $fCO_2^{sw} = 383.01–4.288 \times SST+0.065 \times MLD$ and (B) $fCO_2^{sw} = 384.82–3.579 \times SST–15.021 \times chl\ a+0.055 \times MLD$, plotted versus chlorophyll a (µg L^{-1}). The black line shows the linear regression between the residuals and chlorophyll a.

procedure was used to investigate the influence of MLD as illustrated in Fig. 3A and B. In this case we note that the predicted fCO_2^{sw} is biased low (positive residual) at MLD shallower than 500 m (Fig. 3A), implying that MLD likely contributes to the fCO_2^{sw} algorithm. Fig. 3B shows the residuals when all three of the parameters SST, chl a and MLD are included in the algorithm and we see no correlation with MLD. Adding MLD in the algorithm increased the r^2 from 0.59 to 0.68 and decreased the rms from 14.5 to 12.8 µatm. From this analysis we conclude that both chl a and MLD contribute significantly to improve the fCO_2^{sw} field in our study area during 2005. We explore quadratic, cubic, exponential and logarithmic relationships for MLD and chl a and we find that logarithmic functions of MLD and chl a improve the fit significantly. Olsen et al. (2008) found an exponential relationship between fCO_2^{sw} and chl a, and MLD in a single regression. In our case, logarithmic and exponential functions give the same r^2 and rms. Based on this investigation, we develop two relationships based on observed fCO_2^{sw} (fCO_{2abs}^{sw}), remotely sensed chl a data (20 March–15 October), and SST and MLD from FOAM. Eq. (1) gives the best fit for the period between 20 March and 15 October when satellite chl a data existed and Eq. (2) provides the best fit for the rest of the year. The standard error of each parameter is given in parenthesis after each parameter and N shows the number of data points used in the evaluation. The annual range of fCO_2^{sw} and the independent variables are shown for the two algorithms (Table 2). The units for the parameters are in µatm, °C, µg L^{-1}, and m for, fCO_2^{sw}, SST, chl a, and MLD, respectively.

For 20 March to 15 October, 2005:

$$fCO_2^{sw} = 323.93(\pm1.20) - 2.855(\pm0.062) \times SST - 8.4950(\pm0.161) \times \ln(\text{chl } a) + 10.2161(\pm0.182) \times \ln(\text{MLD})$$
$$N = 13,031, \quad r^2 = 0.72, \quad \text{rms} = 10.9\,\mu\text{atm} \qquad (1)$$

16 October–31 December 2005 and 1 January–19 March, 2005:

$$fCO_2^{sw} = 298.93(\pm0.90) - 0.1678(\pm0.044) \times SST + 14.0385(0.118) \times \ln(\text{MLD})$$
$$N = 6017, \quad r^2 = 0.77, \quad \text{rms} = 5.6\,\mu\text{atm} \qquad (2)$$

The r^2 values of the overall fit indicate how well the algorithm fits the data. There are three factors that may explain the unresolved variance of 28–23%: (1) differences in the temporal and spatial resolution in the field measurements and the remotely sensed and ocean analysis data, (2) uncertainties in the estimated value (the error in NDIR-based seawater fCO_2^{sw} data is generally considered to be ~2 µatm (Pierrot et al., 2008), as well as in predictor variables (FOAM SST and MLD, and MODIS/SeaWiFS chl a data), and (3) processes unrelated to SST, chl a, and MLD affecting fCO_2^{sw}.

Olsen et al. (2008) present the regression diagnostics from single parameters relationships with SST, chl a and MLD. They found that fCO_2^{sw} in the deep basins had poor correlation with SST in winter ($r^2 = <0.01$), and a strong correlation with MLD and chl a in the summer. On an annual basis, the MLD was the best single

predictor for fCO_2^{sw} in the basins and the regression diagnostics for the IcB and IrB were 9.4 and 11.3 μatm and r^2 were 0.81 and 0.71, respectively. This is similar to our results during the March–October period (Eq. (1)), but for the rest of the year, the algorithm is significantly improved by using both SST and MLD (Eq. (2)).

For further discussion on the predictive capacity of MLD, SST, and chl *a* to estimate fCO_2^{sw} the regression coefficients are normalized. The β coefficients are the regression coefficients when all variables are standardized to a mean of 0 and a standard deviation of 1. The advantage of using β coefficients instead of using the non-standardized (or raw regression coefficients, *B*), is that the magnitude of the β coefficients allows for a direct comparison of the relative contribution of each independent variable in the prediction of the dependent variable (i.e. fCO_2^{sw}). In Table 3, we have summarized the beta coefficients (β) for each predictor variable in order to evaluate the relative contribution of each predictor to the overall fCO_2^{sw} prediction for Eqs. (1) and (2). The β coefficients show that chl *a* and MLD both have a larger contribution than SST. For instance, during the winter, when ln(MLD) contributes with 0.87 and SST of 0.03 to the estimated fCO_2^{sw}. The strong ln(MLD) contribution in Eq. (2) is also observed in the improved correlation coefficient (r^2) from 0.18 using only SST, to 0.77 using both MLD and SST and the decreased root-mean-square error (rms) from ±10.6 to ±5.6 μatm, respectively.

We checked the collinearity diagnostics to investigate for unwanted cross-correlation between the independent variables. One possible factor to check for collinearity is to use variance inflation factors (VIF), where a VIF > 5 indicates the presence of cross-correlation between independent parameters (Belsley et al., 1980). Our approach (Eq. (1)) resulted in a VIF for SST, ln(chl *a*), and ln(MLD), of 1.96, 1.46, 1.93, respectively, meaning that our variables do not cross-correlate significantly.

The fCO_2^{sw} algorithms (Eqs. (1) and (2)) were used to compute weekly fields of fCO_2^{sw} in the northern North Atlantic at a resolution of 1° Lat × 1° Lon × 1 week for the region bound by 58°N, 40°W; 58°N, 10°W; 63°N, 40°W; 63°N, 10°W. The ln(chl *a*), SST, and ln(MLD) data were provided at a higher resolution as described above and each parameter was averaged onto the 1° × 1° grid prior to the calculations.

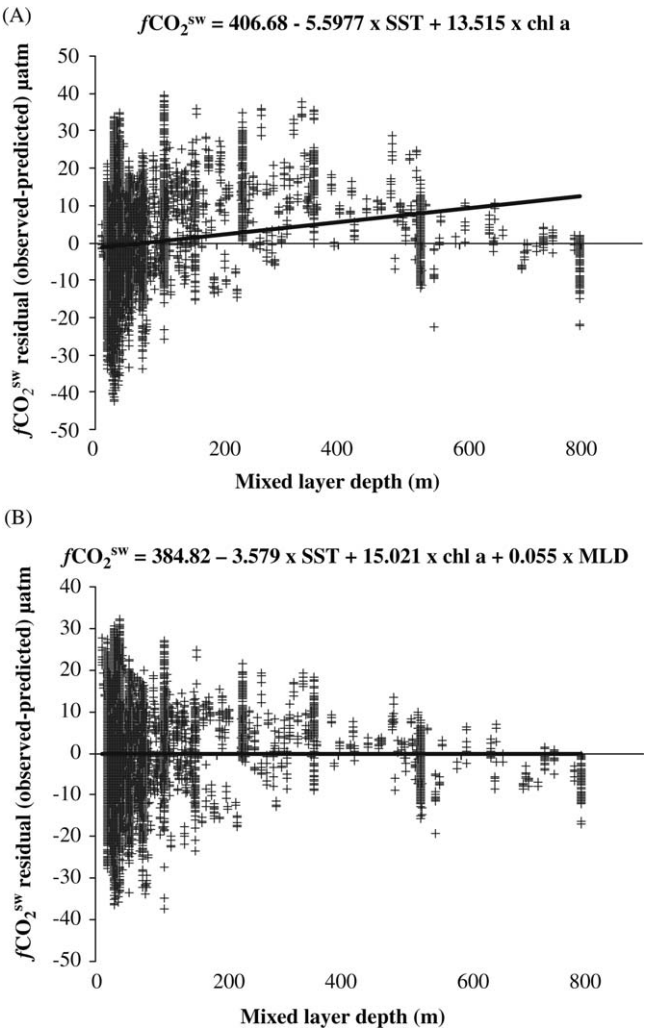

Fig. 3. Residuals (observed−predicted fCO_2^{sw}, μatm) from the equation (A) $fCO_2^{sw} = 414.40 - 5.7563 \times SST - 18.123 \times chl\ a$ and (B) fCO_2^{sw} (SST, chl *a*, MLD), plotted versus MLD (m). The black line shows the linear regression between the residuals and MLD.

4.2. Comparison between observed fCO_2^{sw} and the computed fCO_2^{sw} fields

The measured fCO_2^{sw} data from the *Nuka* were averaged onto the same grid resolution as the fields estimated above, giving a total of 683 bins. The weekly mean residuals of the computed

Table 3
The beta coefficients (β) allow for a comparison of the relative contribution of each independent variable to the overall prediction of the dependent (i.e. fCO_2^{sw}) using Eqs. (1) and (2).

	β (chl *a* period, Eq. (1))	β (no chl *a* period, Eq. (2))
SST	−0.26	−0.03
ln (chl *a*)	−0.30	–
ln (MLD)	0.64	0.87

The β coefficients are regression coefficients, where all variables have been standardized to a value between a mean of 0 and a standard deviation of 1. This makes it possible to compare the relative contribution of each independent variable in the prediction of the dependent variable (i.e. fCO_2^{sw}).

Table 2

	fCO_2^{sw} (μatm)	SST (°C)	chl *a* (μg L^{-1})	MLD (m)
(a) *The range of the* fCO_2^{sw} *and the independent variables (SST, chl a, and MLD) in the data used in Eq.* (1) *for the period* 20 *March*–15 *October*				
Minimum value	283	4.34	0.01	10
Maximum value	391	14.13	4.91	798
Mean	342	9.97	0.66	88
Standard deviation	±20	±2.30	±0.51	±127
(b) *The range of the* fCO_2^{sw} *and the independent variables (SST and MLD) in the data used in Eq.* (2) *for the period* 16 October–19 *March*				
Minimum value	345	4.15	–	57
Maximum value	395	12.19	–	1193
Mean	374	8.40	–	295
Standard deviation	±12	±1.92	–	±204

fCO_2^{sw} (μatm) from algorithms (Eqs. (1) and (2)) and the bin-averaged fCO_2^{sw} data from the *Nuka* are shown in Fig. 4. Negative residuals indicate that the computed values are lower than the measured fCO_2^{sw}. The mean and standard deviation for all residuals for the whole period are 0.5 and ±6 μatm, respectively. The largest bias between the observed and calculated values are observed from week 16 to week 35 (i.e. mid-April to end of August), of −2 μatm (mean value) and a standard deviation of ±8 μatm. In this dynamic period all parameters change rapidly; SST changes abruptly due to surface water warming, the MLD stabilizes, and the onset of biological primary production changes chl *a*. The occurrence of the largest bias in this period is likely due to the different time scales of the expression of these processes on fCO_2^{sw} and parameters such as chl *a* and temperature. The signal of high chl *a* values due to primary production is short lived relative to the timescale of recovery of the depression on fCO_2^{sw} caused by phytoplankton blooms.

4.3. Validation with independent field measurements

An independent validation of the fCO_2^{sw} prediction from our algorithm corresponding to the winter period (from ~October to March, Eq. (2)) was performed by using measured fCO_2^{sw} obtained at the ship R/V *Skogafoss* traveling in the same region during 2005 (Fig. 5). The validation is based on fCO_2^{sw} data measured during five cruises performed in January, February, March, October and November 2005, giving a total number of 8144 data points. The mean residual fCO_2^{sw} between the computed fCO_2^{sw} (Eq. (2)) and the bin-averaged fCO_2^{sw} data from the *Skogafoss* for a total of 64 bins, resulted in a mean of 0.4 μatm and the rms in the computed fCO_2^{sw} is generally within ±10 μatm.

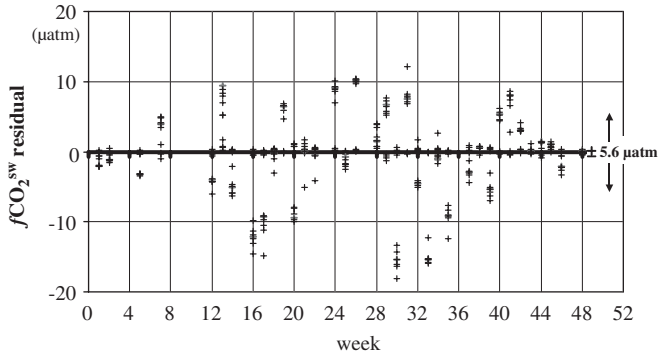

Fig. 4. Weekly mean residuals (predicted−observed) between computed fCO_2^{sw} (Eqs. (1) and (2)) and bin-averaged fCO_2^{sw} data measured onboard the *Nuka*. Resolution is 1° Lat × 1° Lon × 1 week, resulting in a total number of 683 bins. The mean and standard deviation of the residuals were 0.54 μatm, and ±5.6 μatm, respectively.

4.4. Air–sea CO_2 flux calculation

Using the computed fCO_2^{sw} (Eqs. (1) and (2)) we calculated the air–sea CO_2 flux, *F*, according to

$$F = K_0 \times k(fCO_2^{sw} - fCO_2^{air}) \quad (3)$$

where K_0 is the solubility, *k* is the transfer velocity for air–sea CO_2 exchange, and fCO_2^{air} and fCO_2^{sw} are the atmospheric and sea-surface fCO_2, respectively. Solubility was calculated according to Weiss (1974) using the FOAM SST and salinity data.

Weekly mean transfer velocities were calculated according to Wanninkhof (1992):

$$k = 0.31 \frac{\sum U_{10}^2}{n} \left(\frac{Sc}{660}\right)^{-0.5} \quad (4)$$

where U_{10} are the individual Level 2B daily wind-speed retrievals, at a spatial resolution of 25 km from the SeaWinds sensor on the QuickSCAT satellite (obtained at Physical Oceanography Distributed Active Archive Center (PODAAC) at http://podaac.jpl.nasa.gov/). *n* is the number of U_{10} retrievals in each 1° Lat × 1° Lon × 1 week grid cell, and *Sc* is the Schmidt number computed according to Wanninkhof (1992) from the FOAM SST fields. The atmospheric CO_2 data used here were obtained from the Global Monitoring Division Carbon Cycle Greenhouse Gases Group of NOAA/ESRL (http://www.esrl.noaa.gov/gmd/ccgg/index.html). We used linear regression on data of the monthly mean mole fraction of CO_2 in dry air (xCO_2) at Storhofdi, Vestmannaeyjar, Iceland (63.3°N) and Mace Head, Ireland (53.3°N) to obtain the equations describing the latitudinal gradient of monthly mean xCO_2. Using these equations an atmospheric xCO_2 value was determined for each grid cell and the mole fractions were converted to atmospheric CO_2 partial pressure according to

$$pCO_2^{air} = xCO_2(slp - pH_2O) \quad (5)$$

where slp is sea level pressure and pH_2O the partial pressure of water vapor at SST and salinity. Gridded fields of six hourly slp for 2005 were obtained from the NOAA-CIRES Climate Diagnostics Center, Boulder, CO, USA, from their web site at http://www.cdc.noaa.gov/, and originate from the NCEP/NCAR Reanalysis project (Kalnay et al., 1996). The slp data were supplied on a

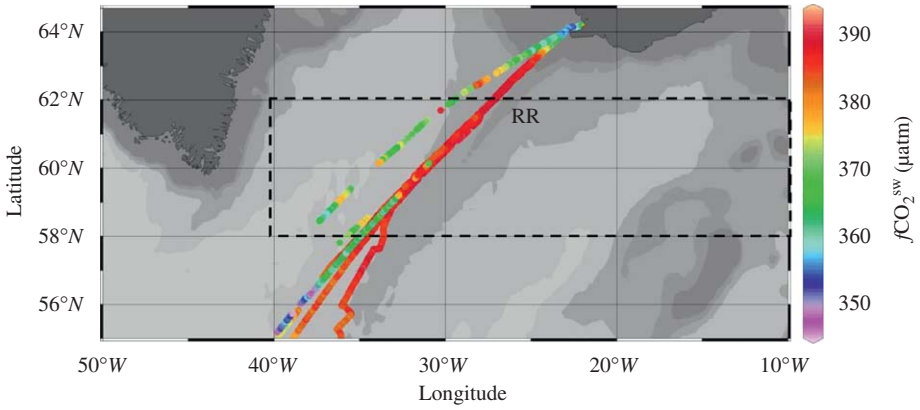

Fig. 5. The location of the fCO_2^{sw} measurements obtained onboard the R/V *Skogafoss* during five cruises in the year 2005 (January, February, March, October and November). The color bar indicates the measured fCO_2^{sw} values (μatm). Note the high fCO_2^{sw} values along the Reykjanes Ridge (RR), measured in November 2005. The dashed rectangle indicates the region for which the validation analysis was performed. The value of the depth contours (m) are indicated by the grayscale bar in Fig. 1.

2.5° Lat × 2.5° Lon grid were re-gridded using a triangle-based cubic spline interpolation to fit the 1° Lat × 1° Lon × 1 week grid size of the fCO_2^{sw} fields. The pH_2O was calculated from FOAM SST after Weiss and Price (1980). The atmospheric pCO_2 was converted to fCO_2^{air} after Weiss (1974), following the procedure described in Dickson and Goyet (DOE, 1994).

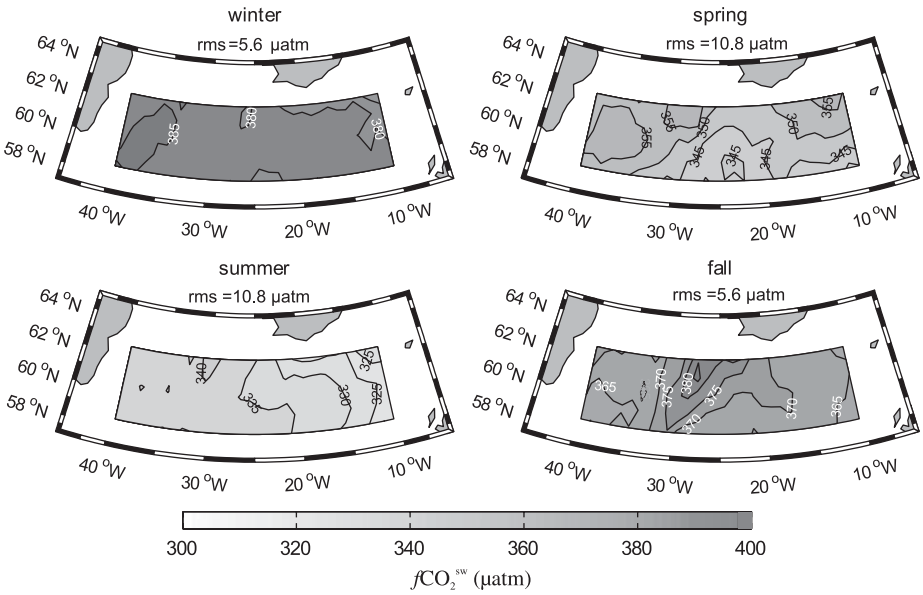

Fig. 6. Seasonal fields of surface water fugacity of CO_2 (fCO_2^{sw}, µatm).

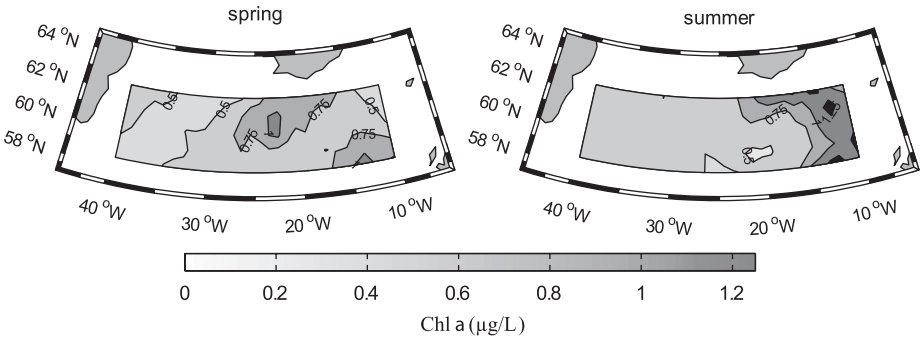

Fig. 7. Seasonal fields of remotely sensed chlorophyll data (chl *a*, $\mu g\,L^{-1}$).

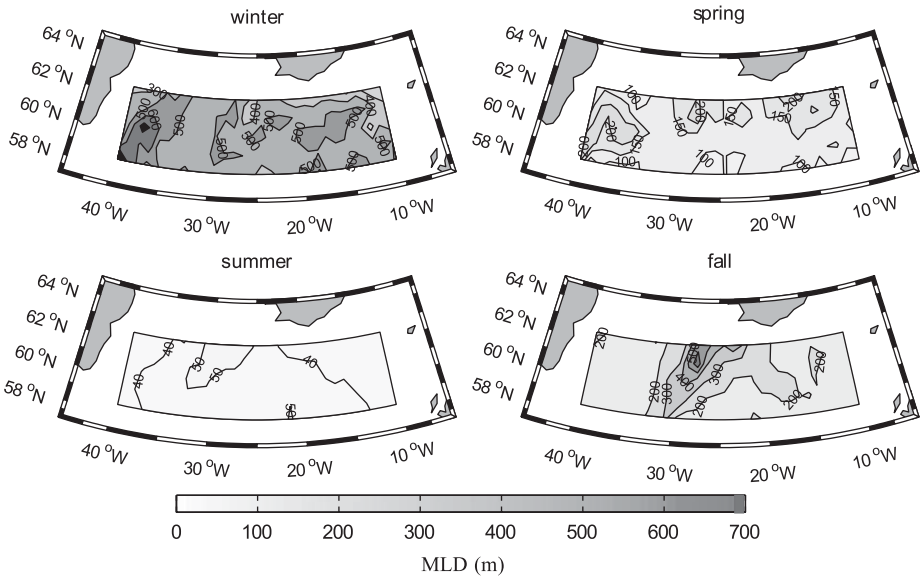

Fig. 8. Seasonal fields of the mixed-layer depth (MLD, m).

5. Seasonal variability of fCO_2^{sw}, chlorophyll, MLD and sea–air CO_2 flux in 2005

We evaluated the seasonal variability by averaging the weekly fCO_2^{sw} fields into four seasons defined as follows; winter: 1 January–19 March (Eq. (2)); spring: 20 March–2 July (Eq. (1)); summer: 3 July–15 October (Eq. (1)), and fall: 16 October–31 December (Eq. (2)). Figs. 6–11 show the seasonal fields of; fCO_2^{sw}, (Fig. 6); chl *a*, (Fig. 7); MLD, (Fig. 8); ΔfCO_2, (Fig. 9); wind speed, (Fig. 10); and sea–air CO_2 flux, (Fig. 11). In winter, we observe relatively constant fCO_2^{sw} values throughout the whole region of about 380 µatm, with slightly higher values in the far west. In spring, fCO_2^{sw} values have decreased relative to winter values, which are due to the biological CO_2 drawdown being larger than the effect of increasing temperatures. The biological CO_2 drawdown continues and fCO_2^{sw} reach lowest values in summer of about 325 µatm in the east, and 340 µatm at about 40°W. The lowest fCO_2^{sw} values in spring and summer coincide with highest chl *a* values (Figs. 6 and 7). Increasing fCO_2^{sw} values are observed in fall, due to the vertical mixing which brings subsurface waters rich in CO_2 to the surface, as the MLD deepens (Fig. 8). Fall fCO_2^{sw} values are typically 370 µatm across the area. However, in the proximity of the Reykjanes Ridge, the fCO_2^{sw} reaches above 385 µatm, which coincides with deeper MLD. This may be a signal of enhanced upwelling over the ridge. High fCO_2^{sw} values of about 390 µatm were also measured along the Reykjanes Ridge onboard the R/V *Skogafoss* in November 2005 (see values in Fig. 5). This suggests that the higher fCO_2^{sw} values along the ridge are real and not an artifact of the algorithm or a limitation of our approach.

The fCO_2^{air} values (not shown) vary from lowest values of 362 µatm in summer to highest values of about 376 µatm in spring. During fall and winter values are about 369 and 374 µatm, respectively.

Winter ΔfCO_2 (Fig. 9) are about 10 µatm supersaturated in the west, and decrease gradually to reach values that are close to

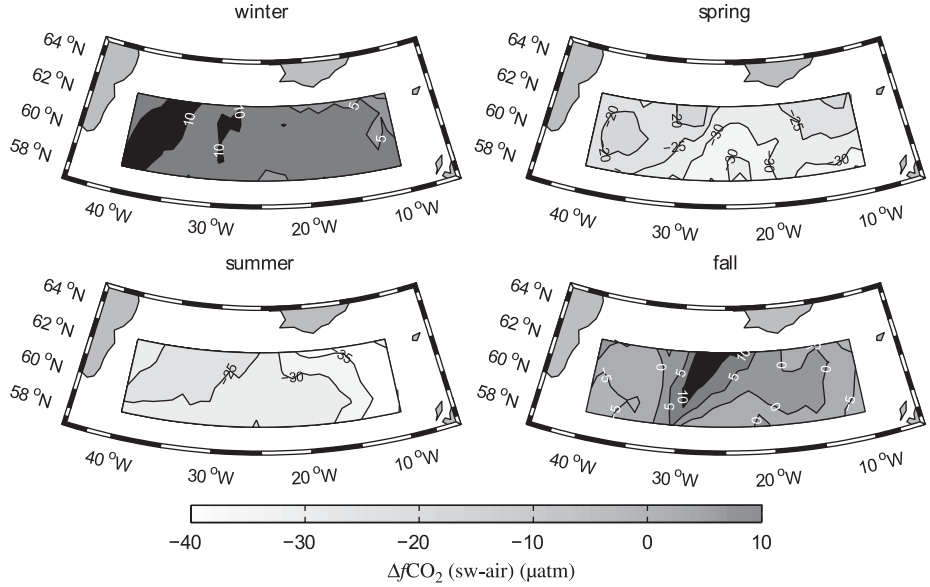

Fig. 9. Seasonal fields of ΔfCO_2 (fCO_2^{sw}–fCO_2^{air}, µatm).

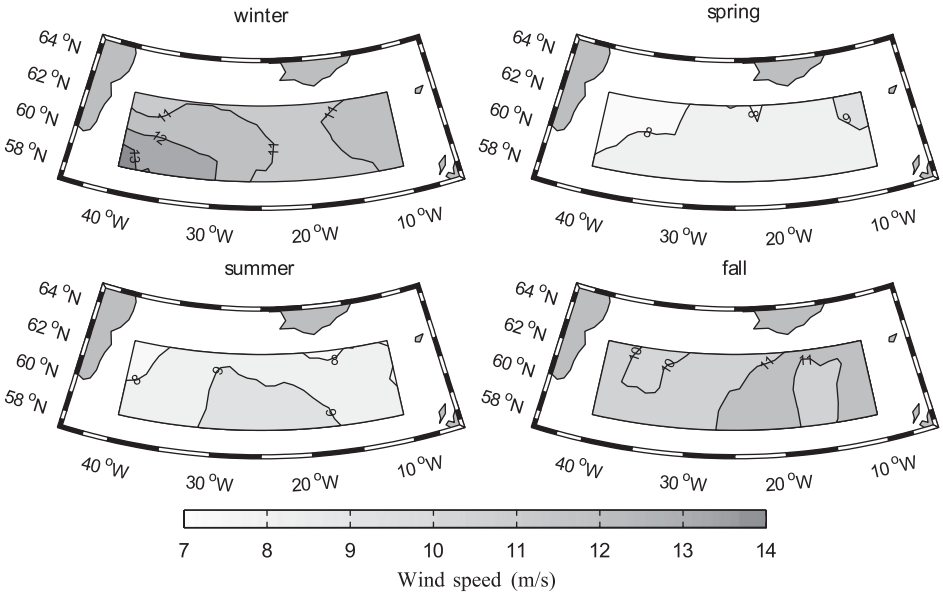

Fig. 10. Seasonal fields of wind speed ($m\,s^{-1}$).

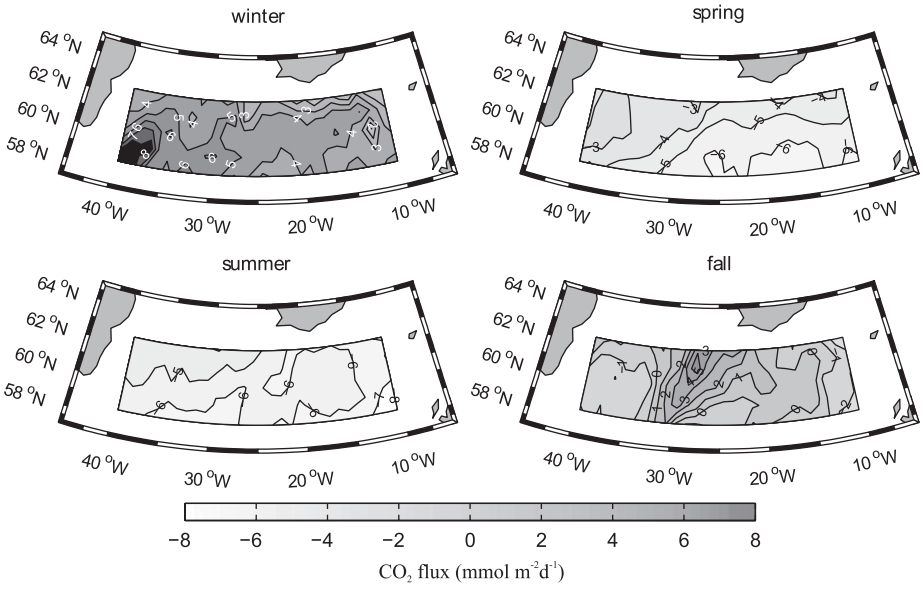

Fig. 11. Seasonal fields of the sea–air CO_2 flux (mmol m^{-2} d^{-1}).

equilibrium with the atmosphere in the eastern part of the study area. The gradual fCO_2^{sw} decrease in spring and summer results in undersaturation ranging from 20 μatm in the western part to 40 μatm in the eastern part. Note that Fig. 9 shows the ΔfCO_2 (fCO_2^{sw}–fCO_2^{air}) so that negative values denote lower values in the ocean than in the atmosphere, thus indicating undersaturated surface water. We observe the largest undersaturation of 40 μatm in the surface water in the eastern area in summer, which is also where we find the highest chl *a* values. The largest supersaturation is observed in fall along the Reykjanes Ridge (RR), and coincides with the deep MLD in this area, as noted above. Except for the feature along the RR, fall values are generally close to the atmospheric CO_2 level.

Fig. 10 shows the remotely sensed wind speed fields. Both the highest and the lowest wind speeds are observed in the western part with wind speeds up to 13 m s^{-1} in winter (southwest) and lowest values of 8 m s^{-1} in spring and summer. The central area has winds ranging from 11 to 8 m s^{-1} with highest wind speeds in winter and fall. In spring and summer wind speeds are uniform and about 8 m s^{-1} in the whole study area.

Fig. 11 shows the seasonal sea–air CO_2 fluxes (mmol m^{-2} d^{-1}), negative values denote an ocean CO_2 sink, and positive values denote an ocean source of CO_2. In winter, we observe outgassing of CO_2 in the whole area, which is most intense in the western part of 6 mmol m^{-2} d^{-1}. This is also where we observe the largest CO_2 supersaturation and the highest wind speeds. On the other hand, in spring and summer the region acts as an oceanic sink of about 6 mmol m^{-2} d^{-1}. Since the wind speed in spring and summer is relatively constant and uniformly distributed, the CO_2 flux pattern follows that of ΔfCO_2. In the fall, we observe the largest variability in the CO_2 flux, and the flux varies from zero to an oceanic CO_2 source of about 4 mmol m^{-2} d^{-1} in the region near the Reykjanes Ridge, which is a result of the high fCO_2^{sw} values at this location during fall. The annual net oceanic across the region uptake was about 5.8 Mt C yr^{-1} (= 0.0058 Gt C yr^{-1}, $M = 10^6$, $G = 10^9$).

6. Conclusion

To obtain a regional CO_2 estimate with a precision of 0.1 Gt C yr^{-1} in the North Atlantic Ocean, the error on regional ΔfCO_2 estimates should not exceed 11 μatm for the region north of 54°N (Sweeney et al., 2002). By using remotely sensed chl *a* data and ocean analysis SST and MLD, we estimated fCO_2^{sw} within ±11 μatm for the period 20 March–15 October. During the rest of the year the estimated fCO_2^{sw} (from MLD and SST) has an estimated accuracy of ±6 μatm. Comparison with independent data indicates an overall accuracy of within ±10 μatm for the winter period (16 October–19 March).

We find that SST, chl *a* and MLD contributed significantly to the estimate of fCO_2^{sw} in our study area. Since little is known about the interannual fCO_2^{sw} variability, and further studies must be carried out to determine the consistency of estimated fCO_2^{sw} from algorithms from year to year. Therefore it is of great importance to continue large-scale international efforts aiming at measuring the fCO_2^{sw} (e.g., Volunteer Observing Ships and buoys) as well as the parameters describing the drivers for the fCO_2^{sw} change. Efforts also should include the development and optimization of remote sensing capabilities both on regional and global scales.

Acknowledgements

This is a contribution to the Swedish Research Council for Environment, Agricultural Sciences and Spatial Planning (Formas Project #2004-797), the REmote Sensing Carbon UptakeE (RESCUE, 96/05) project funded by the Swedish National Space Board, CARBON-HEAT (185093/S30) of the Norwegian Research Council, and the EU IP CARBOOCEAN (GOCE 511176-2). Data from the Skogafoss were provided by Denis Pierrot and Kevin Sullivan of the Cooperative Institute of Marine and Atmospheric Sciences and were funded by the NOAA Climate Observation Division. We are grateful to the owners, captains, officers and the crew of the M/V *Nuka Arctica* of Royal Arctic Lines Denmark and the *Skogafoss* of Eimskip lines, Iceland for their support and participation in the Volunteer Observing Ships (VOS) monitoring program. We are also grateful for comments and questions raised by two reviewers and guest editor Dorothee Bakker which greatly improved the manuscript.

References

Belsley, D.A., Kuh, E., Welsch, R.E., 1980. Regression Diagnostics: Identifying Influential Data and Sources of Collinearity. Wiley, New York.

Boutin, J., Etcheto, J., Dandonneau, Y., Bakker, D.C.E., Feely, R.A., Inoue, H.Y., Ishii, M., Ling, R.D., Nightingale, P.D., Metzl, N., Wanninkhof, R., 1999. Satellite sea surface temperature: a powerful tool for interpreting in situ pCO_2 in the equatorial Pacific Ocean. Tellus 51B, 490–508.

Chierici, M., Fransson, A., Nojiri, Y., 2006. Biogeochemical processes as drivers of surface fCO_2 in constrasting provinces in the North Pacific Ocean. Global Biogeochemical Cycles 20, GB1009.

Cooper, D.J., Watson, A.J., Ling, R.D., 1998. Variation of pCO_2 along a North Atlantic shipping route (UK to the Caribbean): a year of automated observations. Marine Chemistry 72, 151–169.

Cosca, C.E., Feely, R.A., Boutin, J., Etcheto, J., McPhaden, M.J., Chavez, F.P., Strutton, P.G., 2003. Seasonal and interannual CO_2 fluxes for the central and eastern equatorial Pacific Ocean as determined from fCO_2–SST relationships. Journal of Geophysical Research 108 (C8), 3278.

DOE, 1994. In: Dickson A.G., Goyet, C. (Eds.), Handbook of Methods for the Analysis of the Various Parameters of the Carbon Dioxide System in Sea Water; version 2. ORNL/CDIAC-74.

Kalnay, E., Kanamitsu, M., Kistler, R., Collins, W., Deaven, D., Gandin, L., Iredell, M., Saha, S., White, G., Woollen, J., Zhu, Y., Chelliah, M., Ebisuzaki, W., Higgins, W., Janowiak, J., Mo, K.C., Ropelewski, C., Leetmaa, A., Reynolds, R., Jenne, R., 1996. The NCEP/NCAR reanalysis project. Bulletin of the American Meteorological Society 77, 437–471.

Lévy, M., Lehan, Y., André, J-M., Mémery, L., Loisel, H., Heifetz, E., 2005. Production regimes in the northeast Atlantic: a study based on Sea-viewing wide field of view sensor (SeaWiFS) chlorophyll and ocean general circulation model mixed layer depth. Journal of Geophysical Research 110, C07S10.

Lüger, H., Wallace, D.W.R., Körtzinger, A., Nojiri, Y., 2004. The pCO_2variability in the midlatitude North Atlantic Ocean during a full annual cycle. Global Biogeochemical Cycles 18, GB3023.

McCartney, M.S., Talley, L.D., 1982. The subpolar mode waters of the North Atlantic Ocean. Journal of Physical Oceanography 12, 1169–1188.

McClain, C., Hooker, S., Feldman, G., Bontempi, P., 2006. Satellite data for ocean biology, biogeochemistry, and climate research. EOS Transactions, AGU 87 (34), 337–343.

McCulloch, M.E., Alves, J.O.S., Bell, M.-J., 2004. Modelling shallow mixed layers in the northeast Atlantic. Journal of Marine Systems 52, 107–119.

Nakaoa, S.I., Aoki, A., Nakazawa, T., Hashida, G., Morimoto, S., Yamanouchi, T., Yoshikawa-Inoue, H., 2006. Temporal and spatial variations of the oceanic pCO_2 and air–sea CO_2 flux in the Greenland Sea and Barents Sea. Tellus 58B, 148–161.

Nelson, N.B., Bates, N.R., . Siegel, D.A., Michaels, A.F., 2001. Spatial variability of the CO_2 sink in the Sargasso Sea. Deep-Sea Research II 48, 1801–1821.

Olsen, A., Bellerby, R.G.J., Johannessen, T., Omar, A.M., Skjelvan, I., 2003. Interannual variability in the wintertime air–sea flux of carbon dioxide in the northern North Atlantic, 1981–2003. Deep-Sea Research I 50, 1323–1338.

Olsen, A., Triñanes, J.A., Wanninkhof, R., 2004. Sea–air flux of CO_2 in the Caribbean Sea estimated using in situ and remote sensing data. Remote Sensing of the Environment 89, 309–325.

Olsen, A., Brown, K.M., Chierici, M., Johannessen, T., Neill, C., 2008. Sea surface CO_2 fugacity in the subpolar North Atlantic. Biogeosciences 5, 535–547.

Pierrot, D., Neill. C., Sullivan, K., Castle, R., Wanninkhof, R., Lüger, H., Johannessen, T., Olsen, A., Feely, R.A., Cosca, C.E., 2008. Recommendations for autonomous pCO_2 measuring systems and data reduction routines. Deep-Sea Research, this issue [doi:10.1016/j.dsr2.2008.12.005].

Press, W.H., Flannery, B.P., Teukolsky, S.A., Vetterling, W.T., 1986. Numerical Recipes. Cambridge University, Cambridge, UK.

Reynolds, R.W., Rayner, N.A., Smith, T.M., Stokes, D.C., Wang, W., 2002. An improved in situ and satellite SST analysis for climate. Journal of Climate 15, 1609–1625.

Stephens, M.P., Samuels, G., Olson, D.B., Fine, R.A., Takahashi, T., 1995. Sea–air flux of CO_2 in the North Pacific using shipboard and satellite data. Journal of Geophysical Research 100, 13571–13583.

Sweeney, C., Takahashi, T., Gnanadesikan, A., 2002. Spatial and temporal variability of surface water pCO_2 and sampling strategies. In: Appendix D, A Large-Scale CO_2 Observing Plan: In Situ Oceans and Atmosphere (LSCOP), National Technical Information Service, 5285 Port Royal Road Springfield, VA 22161.

Takahashi, T., Sutherland, S.C., Sweeney, C., Poisson, A., Metzl, N., Tilbrook, B., Bates, N., Wanninkhof, R., Feely, R.A., Sabine, C., Olafsson, J., Nojiri, Y., 2002. Global sea–air CO_2 flux based on climatological surface ocean pCO_2, and seasonal biological and temperature effects. Deep-Sea Research II 49, 1601–1622.

Takahashi, T., Sutherland, S.C., Wanninkhof, R., Sweeney, C., Feely, R.A., Chipman, D.W., Hales, B., Friederich, G., Chavez, F., Watson, A., Bakker, D.C.E., Schuster, U., Metzl, N., Inoue, H.Y., Ishii, M., Midorikawa, T., Sabine, C., Hopemma, M., Olafsson, J., Arnarson, T.S., Tilbrook, B., Johannessen, T., Olsen, A., Bellerby, R., de Baar, H.J.W., Nojiri, Y., Wong, C.S., Delille, B., 2008. Climatological mean and decadal change in surface ocean pCO_2, and net sea–air CO_2 flux over the global oceans. Deep-Sea Research, this issue [doi:10.1016/j.dsr2.2008.12.009].

Wanninkhof, R.H., 1992. The relationship between wind speed and gas exchange over the ocean. Journal of Geophysical Research 97, 7373–7382.

Wanninkhof, R., Olsen, A., Triñanes, J., 2007. Air–sea CO_2 fluxes in the Caribbean Sea from 2002–2004. Journal of Marine Systems 66, 272–284.

Watson, A.J., Robinson, C., Robertson, J.E., Williams, P.J.le.B., Fasham, M.J.R., 1991. Spatial variability in the sink for atmospheric carbon dioxide in the North Atlantic. Nature 350, 50–53.

Weiss, R.F., 1974. Carbon dioxide in water and seawater: the solubility of a non-ideal gas. Marine Chemistry 2, 203–205.

Weiss, R., Price, B.A., 1980. Nitrous oxide solubility in water and seawater. Marine Chemistry 8, 347–359.